AGU PUBLICATIONS

JGR

Journal of Geophysical Research: Earth Surface

RESEARCH ARTICLE

10.1002/2014JF003233

Where river and tide meet: The morphodynamic equilibrium of alluvial estuaries

Michele Bolla Pittaluga[1], Nicoletta Tambroni[1], Alberto Canestrelli[2], Rudy Slingerland[2], Stefano Lanzoni[3], and Giovanni Seminara[1]

[1]Department of Civil, Chemical and Environmental Engineering, University of Genoa, Genoa, Italy, [2]Department of Geosciences, Penn State University, University Park, Pennsylvania, USA, [3]Department of Civil, Architectural and Environmental Engineering, University of Padua, Padua, Italy

Key Points:
- Equilibrium bed profile of estuaries exists
- A tidal length identifies the fluvial-marine transition
- Hypersynchronous estuaries cannot be in equilibrium

Correspondence to:
M. Bolla Pittaluga,
michele.bollapittaluga@unige.it

Citation:
Bolla Pittaluga, M., N. Tambroni, A. Canestrelli, R. Slingerland, S. Lanzoni, and G. Seminara (2015), Where river and tide meet: The morphodynamic equilibrium of alluvial estuaries, *J. Geophys. Res. Earth Surf.*, *120*, 75–94, doi:10.1002/2014JF003233.

Received 5 JUN 2014
Accepted 16 DEC 2014
Accepted article online 22 DEC 2014
Published online 22 JAN 2015

Abstract We investigate the morphodynamic equilibrium of tidally dominated alluvial estuaries, extending previous works concerning the purely tidal case and the combined tidal-fluvial case with a small tidal forcing. We relax the latter assumption and seek the equilibrium bed profile of the estuary, for a given planform configuration with various degrees of funneling, solving numerically the 1-D governing equation. The results show that with steady fluvial and tidal forcings, an equilibrium bed profile of estuaries exists. In the case of constant width estuaries, a concave down equilibrium profile develops through most of the estuary. Increasing the amplitude of the tidal oscillation, progressively higher bed slopes are experienced at the mouth while the river-dominated portion of the estuary experiences an increasing bed degradation. The fluvial-marine transition is identified by a "tidal length" that increases monotonically as the river discharge and the corresponding sediment supply are increased while the river attains a new morphological equilibrium configuration. Tidal length also increases if, for a fixed river discharge and tidal amplitude, the sediment flux is progressively reduced with respect to the transport capacity. In the case of funnel-shaped estuaries the tidal length strongly decreases, aggradation is triggered by channel widening, and tidal effects are such to enhance the slope at the inlet and the net degradation of the river bed. Finally, results suggest that alluvial estuaries in morphological equilibrium cannot experience any amplification of the tidal wave propagating landward. Hence, hypersynchronous alluvial estuaries cannot be in equilibrium.

1. Introduction

Estuaries are complex transitional environments, ubiquitously distributed all over the world. They are of enormous societal and environmental relevance. Indeed, estuaries have historically attracted human settlements because they provide accessibility to navigation as well as to fresh water and the fertile soil of the adjacent floodplains. Moreover, the sheltered brackish waters resulting from the mixing of fresh and salt waters provide a unique habitat hosting a variety of animal and vegetal species, favoring biodiversity. The transitional character of these environments makes them vulnerable to the effects of sea level rise and, hence, raises important questions concerning their fate in a century of global warming.

Estuarine morphology results from a number of forcing factors: tidal motion, riverine (i.e., freshwater) flow, wave action, and, possibly, gravitational circulations driven by salinity and density gradients associated with the progressive admixture of river water and seawater [*Hansen and Rattray*, 1966]. Sediment characteristics and local geology can also play a role in shaping an estuary. The mutual interplay and feedbacks of all these physical processes make it difficult to provide a simple agreed classification of these landforms [*Hansen and Rattray*, 1966; *Pethick*, 1984; *Dalrymple et al.*, 1992; *Savenije*, 2005]. It is then not surprising that a number of different classifications have been proposed using different criteria, namely, the estuarine shape, the role of tidal forcing, river forcing, geology, and salinity [*Savenije*, 2005].

According to the evolutionary classification proposed by *Dalrymple et al.* [1992], the planform and altimetric configuration of an estuary are controlled by the relative importance of tides, river outflow, waves, and their variation in time. In the present contribution we focus our attention on the first two forcing mechanisms, not considering the effects of wave actions which can be important in the case of bar-built or microtidal, or coastal lagoon estuaries [*Perillo*, 1995]. We will instead consider the two end members represented by tidally dominated estuaries and river-dominated estuaries, investigating how the transition from one type to the other influences the equilibrium profile. Moreover, as a first approximation, we neglect the role

of possible salinity stratification. A tidally dominated estuary can be defined as an alluvial river (i.e., with movable bed) in which the flow and the morphology are essentially controlled by the tidal propagation which, in turn, is strongly affected both by the tidal range and the estuary geometry. A borderline example of this type of estuary is given by a tidal channel, in which no freshwater and sediment discharges are supplied from upstream. On the other hand, in a river-dominated estuary the freshwater-flowing discharge does not depend on the channel size but is controlled by the aggregation of the flow in the catchment served by the river [*Savenije*, 2005].

In the case of alluvial estuaries, the influence of the freshwater discharge carried out by the incoming river can be crucial in determining the estuary shape. The equilibrium configuration of an alluvial estuary is in general the result of a simultaneous coadjustment of the flow field (driven by river discharge, tidal currents, and, possibly, gravitational circulations) and the altimetric and planform shape of the estuary [*Wright et al.*, 1973; *Pethick*, 1984]. In the seaward portion of the estuary, the flow is typically controlled by the tide, as well as by the geometry of the estuary which, in turn, is a product of the balance between erosional and depositional processes [*Zhou et al.*, 2014]. In the landward, river-dominated portion of the estuary, the meteohydrology of the river catchment determines the fluvial "climate," namely, the sequence of hydrographs and associated sedimentographs which control the channel geometry.

Since the work of *Mirick and Leopold* [1963], the problem of characterizing the hydraulic geometry of an estuary has attracted the interest of a large number of researchers. Initially, the attention concentrated on the hydrodynamics of tide propagation through the estuary [e.g., *Savenije*, 2005, and references therein]. Later on, research shifted toward investigations of the morphodynamic evolution of tidally dominated estuaries toward an asymptotically reached equilibrium configuration. This case, characterized by negligible river discharge, was tackled both numerically [*Lanzoni and Seminara*, 2002; *Todeschini et al.*, 2008; *van der Wegen et al.*, 2010] and analytically [*Schuttelaars and de Swart*, 2000; *Seminara et al.*, 2010; *Toffolon and Lanzoni*, 2010]. On the contrary, much less attention has been paid so far to the case of estuaries in which both the tidal and fluvial forcing concur to the flow field and, hence, the freshwater river flow and its associated sediment discharge play a significant morphodynamic role [*Seminara et al.*, 2012; *Canestrelli et al.*, 2014].

In the present study we investigate this latter case and attempt to construct a rational framework clarifying how the equilibrium morphology of an alluvial estuary responds to the combined actions of tidal and fluvial forcing. As a first step we focus on estuaries with an elongated shape (so that lateral variations of the flow properties are relatively insignificant) and well mixed (such that gravitational circulations play a minor role). A further morphologic ingredient, often observed in nature, is the presence of intertidal areas adjacent to the estuary. We will leave aside the analysis of this feature, which can affect both the hydrodynamics of tide propagation [*Friedrichs and Aubrey*, 1994; *Friedrichs and Madsen*, 1992] and the sediment balance in the estuary. While it will not be too hard to model the former effect in future extensions of the present work, the exchange of sediments between the main channel and the adjacent flats crucially depends on particle resuspension. This process is typically driven by wind waves and deserves attention in the future. We finally neglect Coriolis-driven secondary circulations which, in some circumstances, contribute significantly to sediment dynamics and estuary shaping [*Huijts et al.*, 2009].

Under these assumptions, we seek the equilibrium bed profile of the estuary, for a given planform configuration. We adopt the one-dimensional shallow water continuity and momentum equations, coupled to the one-dimensional sediment balance equation [see *Lanzoni and Seminara*, 2002]. We wish to answer a number of questions. First, what is the morphological response of an alluvial estuary to changes in the tidal range, in the hydrologic regime of the incoming river and in landward sediment supply? Does an equilibrium configuration exist? How can we identify the fluvial-marine transition? What are the possible signatures of the seaward boundary condition on the bed profile in the fluvial zone? All these issues have a crucial importance not only because they control the altimetric profile of the estuary but also because they determine how the facies change along the estuary. Clarifying these issues may thus help in making correct paleoenvironmental and sequence-stratigraphic interpretations of sedimentary successions [*Dalrymple and Choi*, 2007]. We will then explore the role played by the main parameters affecting the contingent equilibrium shape of the estuary, namely, tidal amplitude, freshwater discharge, sediment supply, equilibrium width of the river, and sediment diameter. A wide range of values of parameters appropriate to real estuaries will be explored, varying them separately while keeping the others fixed.

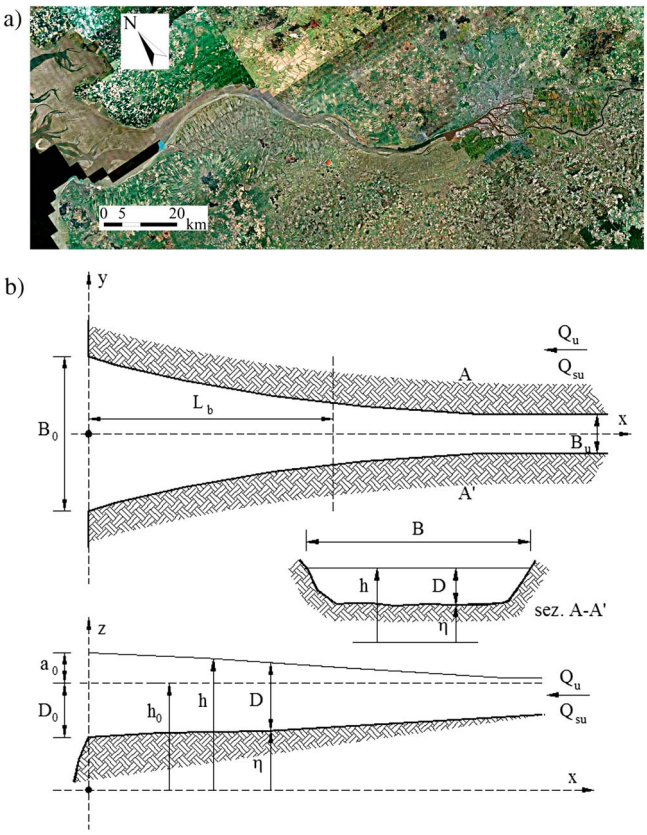

Figure 1. (a) Satellite image of the Elbe Estuary (from Google Earth). (b) Sketch of the investigated domain and notations.

Finally, results will be analyzed in terms of the variation of the tidal range along the estuary. Estuaries are often classified into two classes depending on the spatial amplification of the tidal wave [*Dalrymple and Choi*, 2007]. They are termed "hypersynchronous" when the funnel-shaped channel geometry causes the incoming tide to increase in range because of the progressive decrease in cross-sectional area. Conversely, when bottom friction offsets the influence of convergence, a continual landward decrease in tidal range is observed and the estuary is termed "hyposynchronous." This definition ignores the estuary morphology and is only based on the observations of the hydrodynamics of the tidal wave. Clarifying how the morphological response of the estuary affects its hypersynchronous/hyposynchronous character would ultimately allow for the prediction of the morphological evolutionary tendency of the estuary on the basis of simple measurements of tidal amplification/reduction along the estuary.

The paper is organized as follows. In section 2 we briefly describe the mathematical model, the numerical procedure adopted to solve it, and the conditions imposed at the seaward and landward boundaries. Section 2 also reports the derivation of an analytical asymptotic solution for the case of a tidal amplitude much smaller than the uniform flow depth of the river. Section 3 analyzes the transient process whereby, starting from an initial bed configuration and for given fluvial and tidal forcing, the channel evolves toward some equilibrium configuration. Results are described both for the case of prismatic (constant width) and exponentially varying estuaries. Section 4 argues the issue of the hypersynchronous/hyposynchronous character of tidal propagation in estuaries. In section 5 we report a discussion of the results completed by some suggestions for future research. Finally, section 6 concludes the paper by summarizing schematically the most relevant results.

2. Formulation of the Problem

In this section we formulate the one-dimensional mathematical model used to predict the hydrodynamic and morphodynamic evolution of an estuary.

2.1. Model Description

For the sake of simplicity, the cross section of the estuary is schematized as rectangular, with the width B allowed to vary along the longitudinal direction. Let x denote a longitudinal coordinate with origin at the inlet and pointing landward. We assume that $B(x)$ follows the classic exponential law [e.g., *Langbein*, 1963]. Hence, denoting by B_u the river width asymptotically reached upstream, we write

$$B = B_u + (B_0 - B_u)\exp\left(-\frac{x}{L_b}\right), \tag{1}$$

where L_b is the channel convergence length and B_0 is channel width at the inlet (Figure 1). The bed material is assumed to be composed of uniform sediment, with grain diameter d_s typically set equal to 0.1 mm, unless otherwise stated.

The channel banks are taken to be nonerodible. The estuary planform is then kept fixed when computing the bed profile at equilibrium, an approach widely used in the study of the evolution of tidal channels [*Lanzoni and Seminara*, 2002; *Todeschini et al.*, 2008; *Seminara et al.*, 2010; *Toffolon and Lanzoni*, 2010] and estuaries [*Canestrelli et al.*, 2014]. Essentially, this approach is based on the observation that variations of bed elevation act at a temporal scale typically much smaller than the time scale of width variations.

In the context of a 1-D formulation the fully nonlinear unsteady shallow water equations governing the flow field read as follows:

$$\begin{cases} \dfrac{\partial B(h-\eta)}{\partial t} + \dfrac{\partial Q}{\partial x} = 0 & \text{(2a)} \\ \dfrac{\partial Q}{\partial t} + \dfrac{\partial}{\partial x}\left[\dfrac{Q^2}{B(h-\eta)} + \dfrac{g}{2} B\,(h-\eta)^2\right] = \\ \quad -gBR_h S_f + \dfrac{g}{2}(h-\eta)^2 \dfrac{\partial B}{\partial x} - g\,B\,(h-\eta)\dfrac{\partial \eta}{\partial x} & \text{(2b)} \end{cases}$$

in which h is water surface elevation, η is the laterally averaged elevation of the channel bed, Q is water discharge, R_h is hydraulic radius, and g is gravity. The friction slope S_f reads

$$S_f = \frac{Q^2}{B^2 D^2 k_s^2 R_h^{4/3}} \tag{3}$$

where $D = h - \eta$ is the local instantaneous value of water depth and k_s is the Gauckler-Strickler friction coefficient. The latter coefficient is hereafter set equal to 40 $m^{1/3}$ s^{-1}, unless otherwise stated.

The Exner equation [*Exner*, 1925], governing the bed evolution, reads as follows:

$$\frac{\partial (1-p) B \eta}{\partial t} + \frac{\partial Q_s}{\partial x} = 0 \tag{4}$$

with p as the bed porosity and Q_s as the total sediment load. The latter includes the contributions of both bed load and suspended load and is here computed employing the Engelund-Hansen relationship [*Engelund and Hansen*, 1967]. With the present notation we may write

$$Q_s = 0.05 \left(\frac{Q}{h-\eta}\right)^5 \frac{1}{B^4\, C^3 (g\,\Delta)^2\, d_s} \tag{5}$$

where Δ $(= (\rho_s - \rho)/\rho)$ is the immersed relative density of the bed material, ρ and ρ_s being the density of water and sediment, respectively. Moreover, C is the Chézy conductance coefficient that can be expressed in terms of k_s through the relation $C = k_s R_h^{1/6} g^{-1/2}$.

2.2. Boundary and Initial Conditions

The estuary is fed with some prescribed "formative" freshwater discharge Q_u, as well as with a sediment load Q_{su}. Unless otherwise stated, for a given value of Q_u, the width B_u and the sediment load Q_{su} of the upstream river have been determined through the empirical equilibrium relations derived by *Wilkerson and Parker* [2011] for single-thread sand-bed rivers. Note that the uniform flow conditions embedded by these relations are characterized by an equilibrium bed slope similar to that predicted by employing the Chézy friction relationship and the Engelund and Hansen total load predictor [e.g., *Bolla Pittaluga et al.*, 2014]. A number of simulations have been also carried out by considering nonequilibrium values of either Q_{su} or B_u at the upstream boundary.

Also note that even though the relationships proposed by *Wilkerson and Parker* [2011] have been derived on the basis of observations carried out in sand-bed fluvial rivers, they can reasonably be applied also to the fluvially dominated region of a given estuary, to specify the channel width and upcoming sediment load at the upstream boundary.

At the channel mouth the oscillation of the free surface elevation is imposed by setting

$$h = h_0\,(t) = a_0 \sin(\omega t) \tag{6}$$

with a_0 amplitude of the tidal forcing, $\omega = 2\pi/T$ angular frequency of the tidal wave and T tidal period. The simulations have been performed employing a semidiurnal M_2 tide. The bed elevation at the inlet is free to evolve; however, in the flood phase (flow entering into the estuary) a sediment load in equilibrium with the local hydrodynamics is prescribed, whereas in the ebb phase the sediment load computed at the inlet is

simply assumed to leave the estuary. These conditions are usually employed when modeling tidal channels connected to a large water body, such as a bay, a sea, or an ocean [*Lanzoni and Seminara*, 2002; *Canestrelli et al.,* 2014].

Independently of the planform shape adopted in the analysis (constant width or converging landward), the initial bed profile is assumed to be linear, with a slope, dictated by the river-dominated portion of the estuary, assumed to be in equilibrium with the supplied freshwater discharge and sediment flux. As discussed in *Canestrelli et al.* [2014], for a uniform sediment bed, adopting different initial conditions (e.g., a sloping or a horizontal bed) does not affect the final equilibrium configuration but only influence the time needed to reach equilibrium.

2.3. Morphodynamic Equilibrium

We now define our notion of morphodynamic equilibrium. Based on the Exner equation (4), a tidal channel is in instantaneous morphodynamic equilibrium provided η does not vary in time at any cross section. This condition would strictly require that the instantaneous total sediment flux in the cross section keeps constant everywhere throughout the channel. A weaker form of equilibrium is achieved when the absolute bed elevation does not experience any net variation in a tidal cycle (tidally averaged morphodynamic equilibrium); hence,

$$\eta_{\mathrm{eq}}(x, t+T) = \eta_{\mathrm{eq}}(x, t)\,. \tag{7}$$

This condition implies that equilibrium is achieved provided the net sediment flux in a tidal cycle is constant along the tidal channel and equal to the constant sediment flux delivered by the river. Though in a real estuary the above conditions will never be exactly met as the external forcing to the system (namely, tide oscillations and river discharge) undergo fluctuations, the possible equilibrium attained under steady forcing conditions provides a reference asymptotic state of conceptual relevance.

2.4. The Asymptotic Solution of *Seminara et al.* [2012]

A perturbation solution of the above problem has been recently derived by *Seminara et al.* [2012] under the hypothesis of fairly *small* tidal oscillations at the inlet. As the results of that analysis are relevant to the present context, we think it is appropriate to outline them briefly here. We refer to the above paper readers interested in details of the analysis.

We denote by S, q_u, C_u, and D_u the river bed slope, the prescribed "formative" discharge per unit width of the river, the Chézy conductance coefficient, and the flow depth associated with the uniform flow of the fluvial stream. With the help of the above scaling quantities, we next define the following dimensionless variables:

$$\hat{x} = \frac{Sx}{D_u},\quad \hat{t} = \omega t,\quad (\hat{h}, \hat{D}, \hat{\eta}) = \frac{(h, D, \eta)}{D_u}, \tag{8a}$$

$$\hat{q} = \frac{q}{q_u},\quad \hat{B} = \frac{B}{B_0},\quad \hat{q}_s = \frac{q_s}{\sqrt{\Delta g d_s^3}}. \tag{8b}$$

with the hat denoting a dimensionless quantity.

The governing equations (2a), (2b), (4), and the associated boundary conditions can now be made dimensionless. Note that, in order to make the analysis as simple as possible, the classical Strickler's relationship is employed for the conductance coefficient and the cross section is assumed to be infinitely large. A number of parameters emerge: a dimensionless tidal amplitude $\epsilon = a_0/D_u$, the Froude number of the uniform flow field $F_u = C_u\sqrt{S}$, and the relative rate of width reduction in the upstream direction $\mathcal{B}(\hat{x})$. The latter parameter reads as follows:

$$\mathcal{B}(\hat{x}) = \lambda_b \frac{r_B \exp(-\lambda_b \hat{x})}{1 + r_B \exp(-\lambda_b \hat{x})},\quad r_B = \frac{B_0 - B_u}{B_u},\quad \lambda_b = \frac{D_u}{L_b S}. \tag{9}$$

Recalling the notion of morphodynamic equilibrium and imposing the constraint (7), the dimensionless form of the Exner equation (4) can then be integrated. With the help of the Engelund and Hansen predictor, one finds

$$\exp\left[-\int_{\hat{x}}^{\infty} \mathcal{B}(\hat{x})\mathrm{d}\hat{x}\right] - 1 = < \hat{D}^{-5.5}\hat{q}^5 > \tag{10}$$

where the symbol <> denotes the average over a tidal cycle.

Assuming $\epsilon \ll 1$ and F_u small ($F_u^2 \sim F\epsilon$ with F an $\mathcal{O}(1)$ quantity), the solution can be expanded in powers of ϵ in the following form:

$$(\hat{q}, \hat{D}, \hat{h}, \hat{U}) = (\hat{q}_0, \hat{D}_0, \hat{h}_0, \hat{U}_0) + \epsilon(\hat{q}_1, \hat{D}_1, \hat{h}_1, \hat{U}_1) + \epsilon^2(\hat{q}_2, \hat{D}_2, \hat{h}_2, \hat{U}_2) + \mathcal{O}(\epsilon^3). \tag{11}$$

Substituting from this expansion into the governing equations and equating likewise powers of ϵ, one finds a sequence of differential problems.

The leading order $\mathcal{O}(\epsilon^0)$ problem describes the steady effect of downstream widening on the fluvial stream. This problem is readily solved in closed form and yields

$$\hat{q}_0 = -\exp\left[-\int_\infty^{\hat{x}} \mathcal{B}(\hat{x})\mathrm{d}\hat{x}\right] = -\frac{1}{1 + r_B \exp(-\lambda_b \hat{x})} \tag{12}$$

$$\hat{D}_0 = \hat{q}_0^{8/11}, \quad \hat{h}_0 = \int_0^{\hat{x}} \hat{q}_0^{-14/33}\mathrm{d}\hat{x} \tag{13}$$

The $\mathcal{O}(\epsilon)$ problem describes the propagation of the (small) amplitude tidal wave on the slowly varying fluvial stream. Its solution can be expressed in the following form:

$$[\hat{q}_1, \hat{h}_1] = [0, \hat{h}_{10}(\hat{x})] + [\hat{q}_{11}(\hat{x}), \hat{h}_{11}(\hat{x})][\exp(i\hat{t}) + c.c.] \tag{14}$$

The equilibrium topography of the tidal channel is affected only by the steady component of this solution, namely,

$$\hat{h}_{10} = \frac{F}{2}\left[\left(\frac{1}{1 + r_B}\right)^{6/11} - \left(\frac{1}{1 + r_B \exp(-\lambda_b \hat{x})}\right)^{6/11}\right] \tag{15}$$

The contribution $\delta_1(\hat{x})$ to the depth $\hat{D}_1$ associated with the deviation of bed elevation from the steady $\mathcal{O}(\epsilon^0)$ state is immediately determined by the equilibrium constraint and reads $\delta_1(\hat{x}) = -\hat{h}_{10}(\hat{x})$.

Finally, the differential problem at $\mathcal{O}(\epsilon^2)$ suggests that the steady component of the solution $\hat{q}_{20}$ must again vanish, while $\hat{D}_2$ and $\hat{h}_{20}$ read

$$\frac{\hat{D}_2}{\hat{D}_0} = \frac{20}{11}\frac{<\hat{q}_1^2>}{\hat{q}_0^2} + \frac{143}{44}\frac{<\hat{D}_1^2>}{\hat{D}_0^2} - 5\frac{<\hat{q}_1\hat{D}_1>}{\hat{q}_0\hat{D}_0} \tag{16}$$

$$\hat{h}_{20} = \int_0^{\hat{x}} \left[-\frac{167}{33}\hat{q}_0^{-80/33} < \hat{q}_1^2 > -\frac{65}{18}\hat{q}_0^{-62/33} < \hat{D}_1^2 > \right. \tag{17}$$

$$\left. +10\hat{q}_0^{-71/33} < \hat{q}_1\hat{D}_1 > \right] \mathrm{d}\hat{x} \tag{18}$$

It is worth noting that, as $\hat{x} \to \infty$, $\hat{D}_2 \to 0$, hence $\hat{h}_{20}|_{\hat{x}\to\infty}$ tends to $(-\delta_2)|_{\hat{x}\to\infty}$. These quantities do not vanish and turn out to be negative: they essentially set the elevation of the fluvial stream bed relative to the mean sea level at equilibrium.

2.5. Numerical Solution for Finite Relative Tidal Amplitudes

The analytical solution just described strictly holds when the ratio of the tidal amplitude to the uniform flow depth, ϵ, and the river Froude number, F_{ru}, are both small. The general morphodynamic behavior of an estuary then needs to be explored through a numerical solution of the system of partial differential equations (2a), (2b), and (4).

The numerical procedure requires particular attention. Indeed, in order to ensure mass conservation with an acceptable accuracy in the context of long-term simulations, the numerical scheme must ensure mass conservation and satisfy the so-called well-balanced property, whereby a quiescent steady state is reproduced with sufficient accuracy by the numerical algorithm [*Canestrelli et al.*, 2009, 2010, 2012; *Canestrelli and Toro*, 2012].

The numerical scheme should be effective also in the presence of strong channel convergence and high amplitude tides, when a tidal bore can form. A tidal bore essentially consists of a discontinuity of the water surface elevation (and of the flow speed) which travels in the landward direction. In order to capture the possible formation of this front with the related variations of bed elevation, we use the PRICE-C scheme, with

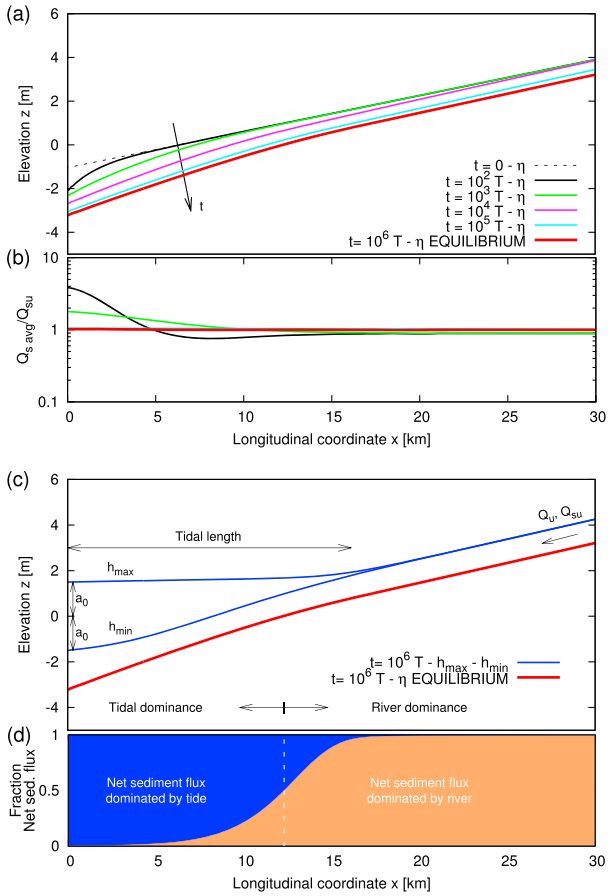

Figure 2. The transient process toward the equilibrium configuration of a constant width estuary, starting from a sloping bed in equilibrium with the upstream river discharge and sediment flux. (a) Temporal evolution of the bed profile. (b) Temporal evolution of the ratio between the net sediment flux and the fluvial flux, showing that, approaching equilibrium, this ratio tends to 1 uniformly throughout the estuary. (c) The equilibrium configuration. (d) Distribution of the fraction of net (tidally averaged) sediment flux due to the tidal currents and the river flow at equilibrium. The net sediment flux due to the river flow has been calculated with equation (5) employing the values of the net flow discharge and the tidally averaged flow depth. The values of the relevant input data employed in this simulation are $d_s = 0.1$ mm, $Q_u = 100$ m^3/s, $Q_{su} = 0.0071$ m^3/s, $B_u = 182$ m, and $a_0 = 1.5$ m.

the modifications introduced by *Canestrelli et al.* [2014] which ensure mass conservation and well balancing of fluxes and source terms also for nonprismatic cross sections.

Finally, taking advantage of the observation that the hydrodynamic time scale is usually much smaller than the morphodynamic time scale, we decouple the two processes and introduce a "morphological factor" (MF) to speed up the computation of the variations of bed elevation. We refer the interested reader to *Roelvink* [2006] for details on the use of the morphological factor in tidal computations.

3. Results

3.1. Transient Evolution Toward Equilibrium of Tidal Channels

In order to introduce the reader to our numerical simulations, it is preliminarily convenient to recall briefly the main features of the transient process whereby, starting from some initial state, a tidal channel, with no water and sediment discharges supplied from upstream, evolves toward some asymptotically reached equilibrium state.

The evolutionary scenario emerging from both numerical investigations [*Lanzoni and Seminara*, 2002; *Todeschini et al.*, 2008] and laboratory observations [*Tambroni et al.*, 2005] is characterized by the progressive landward migration of a sediment wave, whereby the bed degrades seaward and aggrades landward, eventually leading to the formation of a shore. The channel adjusts its length and its longitudinal bed profile until an equilibrium configuration is asymptotically reached, satisfying the constraint of vanishing residual (i.e., tidally averaged) sediment flux at any cross section. Indeed, it turns out that coupling the bed morphology to the flow field leads to a progressive decrease of the tidal flow asymmetry and hence of the residual sediment flux. The final equilibrium state is characterized by a nearly constant value of the maximum flood/ebb speed along the channel, implying a power law relationship between the minimum cross-sectional area and the corresponding tidal prism [*Friedrichs*, 1995; *Lanzoni and Seminara*, 2002; *Tambroni and Seminara*, 2009; *D'Alpaos et al.*, 2010].

In the case of short tidal channels with a small relative tidal amplitude, *Seminara et al.* [2010] have shown analytically that, at equilibrium, the maximum flow speed must coincide with the threshold speed for sediment motion. Whether this stricter condition must hold for tidal channels with arbitrary length is a matter to be explored, which however falls outside the scopes of the present work. Obviously, channel convergence also plays a role. In the fixed bed case, it is known that, depending on its magnitude relative to friction, it may determine either amplification or damping of the tidal wave, enhancing its distortion (see, among others, *Jay* [1991], *Friedrichs and Aubrey* [1994], *Lanzoni and Seminara* [1998], and *Savenije and*

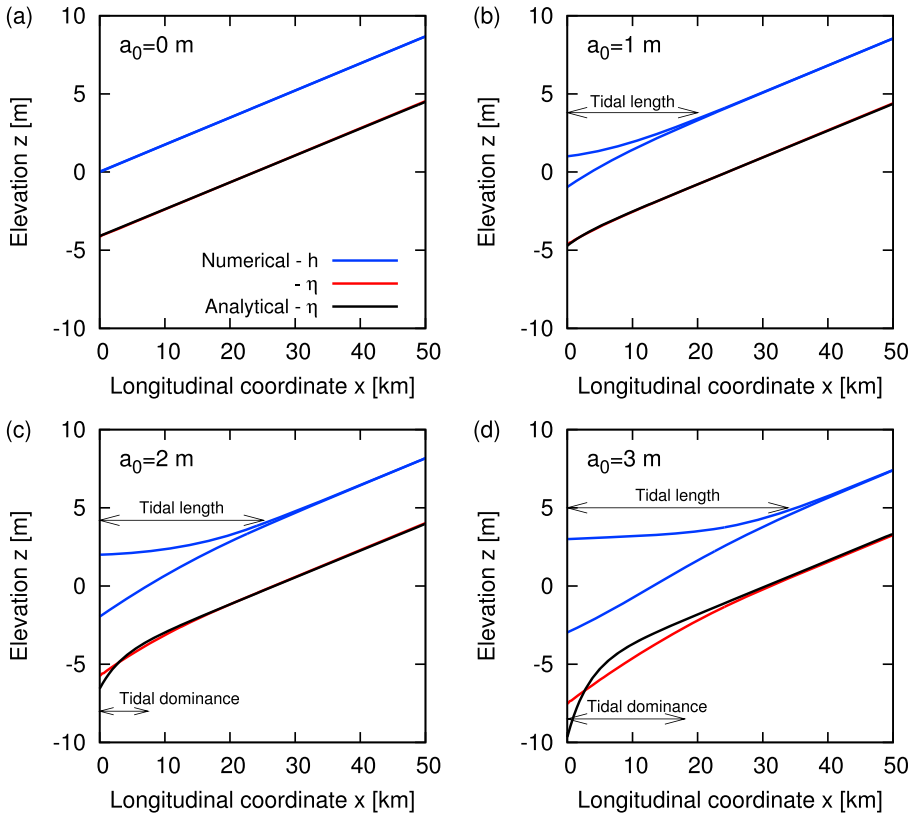

Figure 3. Equilibrium morphology of a constant width estuary for different values of the tidal amplitude: (a) $a_0 = 0$ m, (b) $a_0 = 1$ m, (c) $a_0 = 2$ m, and (d) $a_0 = 3$ m. Red lines denote the longitudinal equilibrium bed profile; black lines are analytical predictions (equation (11)); blue lines are the envelopes of the maximum and minimum values of free surface elevation along the estuary. We have adopted values of the river width and sediment transport rate related to the freshwater river discharge through the *Wilkerson and Parker* [2011] relationship appropriate for single-thread sand-bed rivers. Input data: $d_s = 0.1$ mm, $Q_u = 1000$ m^3/s, $Q_{su} = 0.355$ m^3/s, $B_u = 182$ m.

Veling [2005]). However, in the mobile bed case, the work of *Seminara et al.* [2010] suggests that no tidal amplification may survive at equilibrium.

In the following sections, this well-established scenario will be extended to the estuarine case, including the additional nontrivial effect of water and sediment discharges supplied by the river.

3.2. Results for Constant Width Estuaries

We first concentrate our attention on the case of estuaries with constant width B_u. Although this planform shape is quite uncommon in natural channels [*Savenije*, 2005], considering it as a first step in our analysis allows us to investigate the interaction between river flow and tidal propagation separating the effect of channel convergence. Moreover, a movable river bed with a constant width cross section throughout its length can exist when an artificial diversion is performed, with banks strengthened in order to prevent lateral erosion.

3.2.1. Transient Evolution Toward Equilibrium of Estuaries

Figure 2 reports the results of a simulation where, starting from an initial uniformly sloping bed, equilibrium is progressively attained. Owing to the tidal flow, a scour initially develops near the inlet section and then progressively propagates upstream (Figure 2a) until the net sediment flux along the estuary equals that supplied from upstream (Figure 2b). The final equilibrium configuration is characterized by two distinct regions along the estuary (Figure 2c): a steeper seaward reach, dominated by the tide, along which the tidal amplitude is progressively damped and the envelope of the maximum free surface elevation is approximately horizontal; an upstream fluvial reach, dominated by the river, characterized by the undisturbed bed slope. Although the fluvially dominated reach is not directly affected by the tidal wave, however, its equilibrium bed elevation relative to the mean sea level is affected by the tidal motion, in accordance

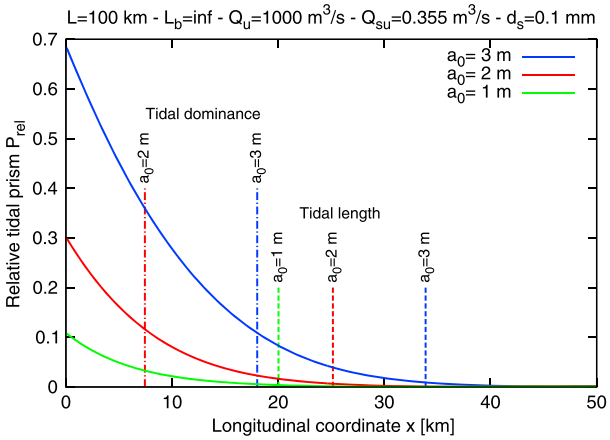

Figure 4. Along-channel distribution of the relative tidal prism for a constant width estuary and three different values of tidal amplitude at the mouth. The vertical lines indicate the values of the tidal length and of the tidal dominance for different tidal amplitudes at the mouth. The relevant input data are the same as in Figure 3.

with the analytical solution recalled in section 2.4. Numerical results in fact show that the initial configuration of the fluvial reach undergoes degradation. The extension of the tide-dominated region (tidal length in Figure 2c) is defined here as the distance from the estuary inlet where the tidal amplitude a is reduced to a 5% of the forcing amplitude a_0. The distinction between the tide-dominated and the river-dominated regions of the estuary is also apparent in Figure 2d, showing how the fractions of net (tidally averaged) sediment flux due to the tidal currents and the river flow are distributed along the estuary. Below, we employ the expression "tidal dominance" to define the length of the region of the estuary where the fraction of the net sediment flux driven by the tidal currents is larger than 50% of the total net sediment flux.

3.2.2. Effect of Tidal Amplitude

Results of simulations performed varying the tidal amplitude at the estuary mouth are shown in Figure 3. In the absence of any tide (Figure 3a), the equilibrium configuration obtained at the end of the simulation is characterized by a uniform flow on a constant slope exactly equal to the slope predicted employing the Chézy relationship and the *Engelund and Hansen* [1967] total load predictor [*Bolla Pittaluga et al.*, 2014]. Increasing the amplitude of the tidal oscillation leads to a progressively higher bed slope at the mouth, as well as to an increasing bed degradation in the river-dominated portion of the estuary (Figures 3b–3d). We also observe that the asymptotic solution given by equation (11) predicts correctly the estuary profile for small enough values of the relative tidal amplitude ϵ while, as expected, a progressive deviation from the numerical solution occurs as ϵ increases. The transition from the tidally dominated to the river-dominated region of an estuary is also apparent from the along-channel distribution of the relative tidal prism P_{rel}, defined as the ratio between the volume of water flowing through a given cross section in half a tidal cycle, decreased by the fluvial component, and the volume of freshwater supplied from the river in the same amount of time:

$$P_{rel} = \frac{\int_t^{t+T/2} |Q(\tau)| d\tau - Q_u T/2}{Q_u T/2} \quad (19)$$

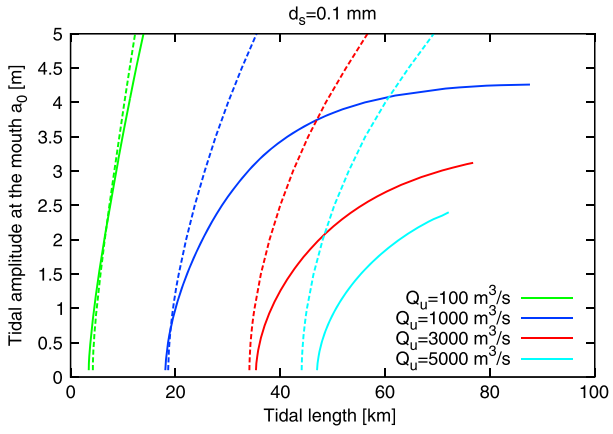

Figure 5. Variations of the tidal length as a function of the tidal amplitude for a constant width estuary and four different values of the river discharge ($Q_u = 100\ m^3/s$, green line; $Q_u = 1000\ m^3/s$, blue line; $Q_u = 3000\ m^3/s$, red line; and $Q_u = 5000\ m^3/s$, light blue line). Dashed lines refer to the flow field obtained by forcing with progressively larger tides the initial uniform bed configuration, assumed to be fixed. The river width and the sediment discharge prescribed at the landward boundary have been chosen according to the equilibrium relationships of *Wilkerson and Parker* [2011].

The spatial distribution of P_{rel} corresponding to the equilibrium profiles of Figure 3 is plotted in Figure 4. It confirms that the tidal influence progressively decreases with distance from the mouth. If the notion of tidal length is based on the distance from the inlet where $P_{rel} = 0.05$ (instead of $a/a_0 = 0.05$), then slightly shorter values are found.

Figure 5 summarizes the effect of tidal amplitude on tidal length. For each value of Q_u, many simulations have been performed with different values of a_0.

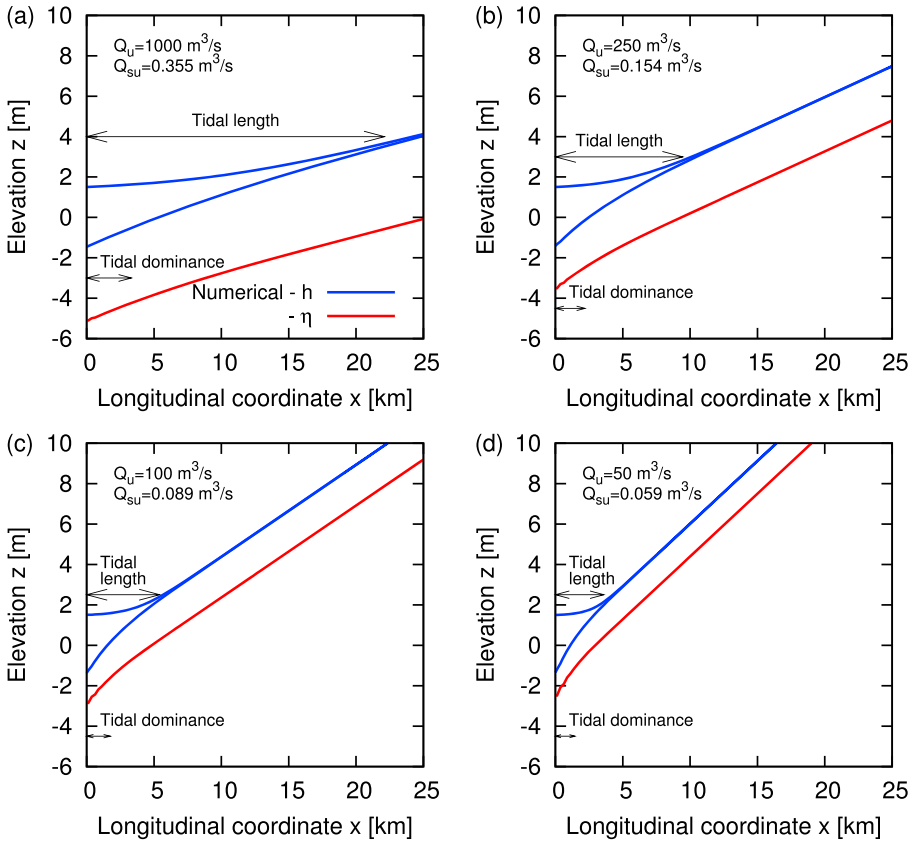

Figure 6. Equilibrium morphology of a constant width estuary for a prescribed tide (a_0 = 1.5 m) and different values of the upstream river discharge: (a) $Q_u = 1000\,m^3/s$, (b) $Q_u = 250\,m^3/s$, (c) $Q_u = 100\,m^3/s$, and (d) $Q_u = 50\,m^3/s$. Sediment size: $d_s = 0.1$ mm. The corresponding sediment transport rates, computed by the empirical formula of *Wilkerson and Parker* [2011] are $Q_{su} = 0.355\,m^3/s$, $Q_{su} = 0.154\,m^3/s$, $Q_{su} = 0.089\,m^3/s$, and $Q_{su} = 0.059\,m^3/s$, respectively. Red lines denote the longitudinal equilibrium bed profile; blue lines denote the maximum and minimum values of free surface elevation along the estuary, respectively.

Not surprisingly, as the forcing amplitude increases, the tidal length increases quite rapidly. However, for a given river discharge, a limiting value of a_0 exists (e.g., about 4.2 m for $Q_u = 1000\ m^3/s$ and 3.2 m for $Q_u = 3000\ m^3/s$) for which the equilibrium length of the estuary (and hence the size of the tide-dominated region) increases abruptly. As we will show later (section 4), such limiting condition corresponds to the attainment of a configuration where the tidal range is kept approximately constant in the seaward portion of the estuary. In the case of a fixed bed with linear slope (represented by the dashed lines in Figure 5) we note that the tidal length increases more slowly with the tidal amplitude and no threshold amplitude appears to exist. The different behavior observed for fixed and movable bed conditions is related to the fact that in the latter case, larger flow depths are generated and frictional dissipation, responsible for tidal wave damping, decreases.

3.2.3. Effect of River Flow Discharge, Sediment Supply and River Width

Figure 6 reports the equilibrium profiles obtained fixing the tidal forcing (a_0 = 1.5 m) and decreasing the river discharge. In the following, we consider as reference equilibrium configuration that obtained for a river discharge $Q_u = 1000\ m^3/s$. For the fluvial-dominated reach it appears that lower freshwater discharges are associated with larger bed slopes and smaller flow depths. This is a direct consequence of the empirical relations of *Wilkerson and Parker* [2011] employed to prescribe the upstream river width and sediment transport rate. The equilibrium bed slope, in fact, is proportional to the −0.394 power of the flow discharge. Consequently, for a prescribed tidal amplitude, the region where tidal effects are felt decreases as the river discharge decreases.

The results of the simulations considered so far are summarized in Figure 7, where the value of the tidal length at equilibrium is plotted as a function of the river discharge Q_u supplied upstream. When

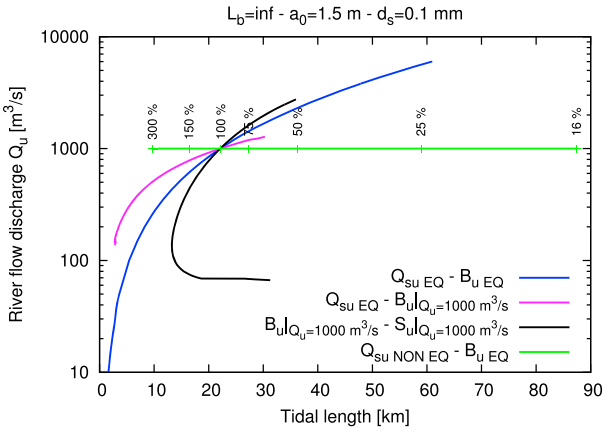

Figure 7. Summary of the tidal length dependence of the upstream river discharge Q_u for a constant width estuary, a tidal amplitude $a_0 = 1.5$ m and different values of the upstream sediment supply, river slope, and width. Blue line: sediment flux and upstream river width computed through the equilibrium relationships of *Wilkerson and Parker* [2011] (see Figure 6); purple line: fixed river width, equal to the equilibrium value for a discharge of 1000 m^3/s; black line: river width and river slope in equilibrium with a flow discharge of 1000 m^3/s; green line: upstream sediment flux progressively reduced or increased with respect to the equilibrium value (see Figure 8).

Q_u and the related sediment supply Q_{su} increase, the limit of the tidally influenced region progrades landward monotonically, independently of whether the river width is kept fixed (purple line) or is prescribed to be in equilibrium with the fluid discharge (blue line). Conversely, a nonmonotonic trend is found when the freshwater discharge is varied while the width and slope of the river are kept fixed (black line). In this latter case an intermediate value of Q_u exists for which the tidal length attains a minimum. Decreasing the flow discharge below this value (which, in the simulation discussed here, is approximately equal to $Q_u = 50$ m^3/s) the tidal length undergoes an abrupt increase. As already pointed out, such threshold condition corresponds to an equilibrium configuration where the tidal range is spatially constant in the seaward portion of the estuary. Note, however, that when the tidal length becomes fairly long (say larger than 100 km) a number of additional effects, not considered here, should in principle be accounted for. They include the downstream fining of sediment, the longitudinal variation of river flow discharge and sediment flux due to tributaries that determine the concave up longitudinal profile of the river bed. In addition, some geological constraints might control the bed erosion along the estuary, thus limiting the tidal length increase. On the other hand, for a fixed river discharge (green line), a progressive reduction (increase) of the sediment flux with respect to its equilibrium value leads to an increasing (decreasing) extension of the tidally influenced region. A similar trend is obtained by varying the relative width of the river with respect to its equilibrium value in the fluvial reach (Figure 8).

3.2.4. Effect of Grain Size, Friction Coefficient, and Length of the Computational Domain

Trends similar to those just described are obtained if the grain size or the friction coefficient is varied with respect to the reference case. More specifically, Figure 9 shows that the equilibrium slope in the fluvial reach increases with increasing values of sediment size, consistent with the relation of *Wilkerson and Parker* [2011], which predicts a dependence of the equilibrium bed slope on sediment size to the power of 0.691. As a consequence, river velocity and tidal dissipation increase with grain size, leading to a shorter tidal length at equilibrium. Figure 10, on the other hand, shows that in varying significantly the friction coefficient, the variation of tidal length is minimal. This result is mainly due to the mild dependence of the equilibrium bed slope on k_s (i.e., to the power of 2/11, see equations (3) and (5)). In addition, the increase of k_s determines an increment of the velocity and reduces the depth in the riverine reach. As a consequence, the reduction of the conductance attained for larger k_s is approximately counteracted by the depth reduction in

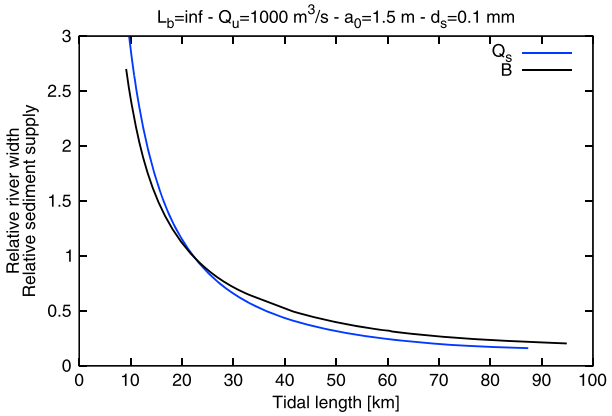

Figure 8. Tidal length variations for fixed values of tidal amplitude ($a_0 = 1.5$ m) and freshwater river discharge ($Q_u = 1000$ m^3/s) as the relative upstream sediment supply Q_s/Q_{su} or the relative river width B/B_u vary. The equilibrium values associated with the imposed river discharge are $Q_{su} = 0.355$ m^3/s and $B_u = 182$ m.

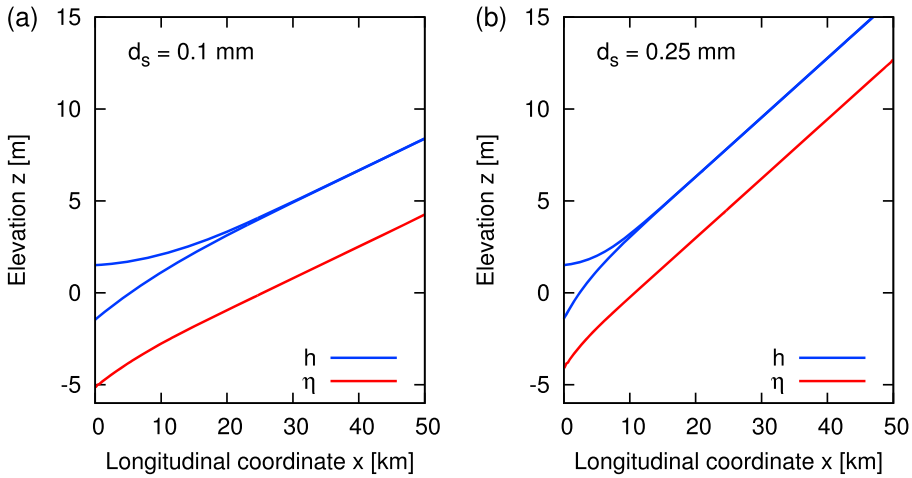

Figure 9. Effect of change in sediment size. Note that, with an increase of sediment diameter, both the sediment flux from upstream and river width slightly increase owing to the *Wilkerson and Parker* [2011] relations employed to specify the upstream boundary conditions. Input data: $Q_u = 1000\ m^3/s$, $a_0 = 1.5$ m. (a) $d_s = 0.1$ mm, $Q_{su} = 0.355\ m^3/s$, $B_u = 182$ m. (b) $d_s = 0.25$ mm, $Q_{su} = 0.370\ m^3/s$, $B_u = 194$ m.

the estuary. By comparing Figure 10a with Figure 10b, in which the tide is absent, it can be appreciated that the higher depth at the mouth for a larger k_s is mainly due to the smaller depth of the uniform equilibrium flow. The tide simply leads to an increase of the depth by an amount which is almost independent of k_s.

Finally, we wanted to examine how the size of the computational domain affects the morphodynamic equilibrium. We performed a further set of simulations fixing the external constraints ($a_0 = 4.0$ m, $Q_u = 1000\ m^3/s$, $Q_{su} = 0.355\ m^3/s$, $L_b = \infty$) and varying the length of the computational domain. The results are plotted in Figure 11. They show that flow discharge and sediment flux are strongly affected by the tide at the landward boundary if the length of the computational domain is too short ($L = 20$ km). In this case, the equilibrium configuration differs significantly from the correct one, which is obtained adopting a sufficiently long computational domain ($L = 100$ km). In order for the solution to be independent of the domain length, the upstream boundary should extend up to the riverine reach, i.e., it should be placed upstream from the point where the bed slope and the water depth at equilibrium attain the values of the uniform river flow. All the simulations in this paper has been run with an upstream boundary falling in the riverine reach, and sometimes a trial and error approach has been necessary in order to satisfy the latter constraint.

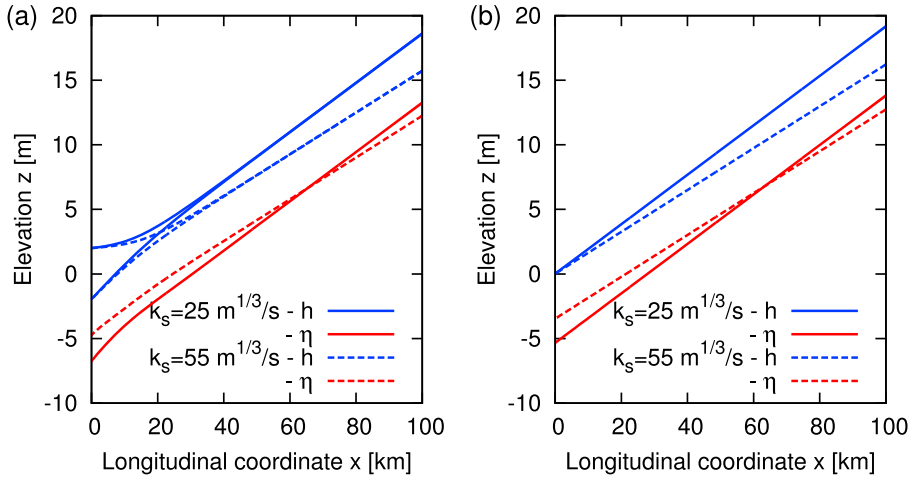

Figure 10. Effect of change in friction coefficient k_s. Input data: $d_s = 0.1$ mm, $Q_u = 1000\ m^3/s$, $Q_{su} = 0.355\ m^3/s$, $B_u = 182$ m. (a) $a_0 = 2$ m. (b) $a_0 = 0$ m.

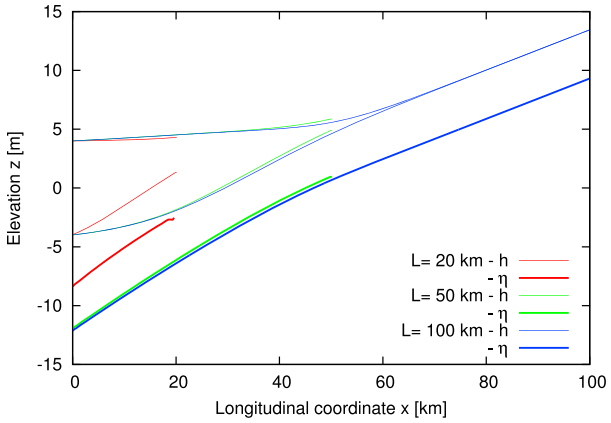

Figure 11. The effect of the length of the computational domain on the equilibrium profile of a constant width estuary emerges from results of a set of simulations performed assuming the following external constraints: $a_0 = 4.0$ m, $Q_u = 1000$ m^3/s, $Q_{su} = 0.355$ m^3/s, $L_b = \infty$ and choosing various lengths L of the computational domain: red lines, $L = 20$ km; green lines, $L = 50$ km; blue lines, $L = 100$ km.

3.3. Results for Convergent Estuaries

Let us now move to the more commonly observed case of convergent estuaries. The planform configurations analyzed in the various tests have been obtained from equation (1) by either varying the convergence length L_b, keeping fixed the widths B_0 and B_u (Figure 12a), or fixing the convergence length and varying the ratio r_B defined in equation (9) for a given value of the upstream river width B_u (Figure 12b).

Figure 13a shows the equilibrium bed profiles calculated for different values of L_b with a prescribed value of r_B, in the limiting case of purely fluvial conditions ($a_0 = 0$). The picture emerging from this figure confirms the recent findings of *Bolla Pittaluga et al.* [2014]: at equilibrium, alluvial channels react to narrowing or widening of the cross section by modifying the flow depth and the bed profile so as to keep the total sediment discharge constant. In particular, widening channels at equilibrium experience a progressive seaward decrease of the free surface as well as a bed aggradation associated with sediment deposition, leading to a reduction of the flow depth.

Figure 13b shows that the above picture is modified when a tidal oscillation is forced at the inlet. Bed aggradation is still driven by channel widening, but owing to tidal currents, the flow deepens and the bed profile lowers, an effect which extends upstream involving the riverine reach. The amount of this degradation is not significantly affected by the rate of channel convergence, at least within the range of values investigated here.

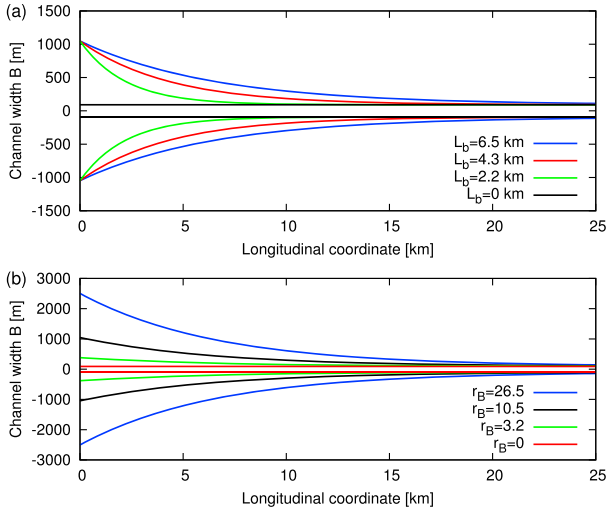

Figure 12. Typical examples of estuary planforms investigated in the present numerical tests. (a) The width of the estuary mouth B_0 and of the upstream river section B_u are kept fixed ($B_0 = 2093$ m, $B_u = 182$ m, $r_B = 10.5$) while the convergence length L_b is varied. (b) The convergence length is kept fixed ($L_b = 6.5$ km) while the ratio $r_B = (B_0 - B_u)/B_u$ is varied for a constant value of the upstream river width B_u ($B_u = 182$ m).

Similar conclusions can be drawn from results of simulations performed for the planform geometries reported in Figure 12b, characterized by a fixed convergence length and different values of the relative width of the estuary inlet. The analogies between purely fluvial and mixed tidal-fluvial conditions are again strong (Figures 14a and 14b). The shape of the bed profiles are qualitatively similar in the two sets of simulations, with some differences in the near-inlet region where, in the tidal case, the bed invariably develops a concave down profile, the flow deepens and, again, the bed profile lowers throughout both the tidal-dominated and the fluvial-dominated reaches. Note that in a prismatic channel the slope increases monotonically downstream, thus leading to an invariantly concave down profile throughout the estuary (see, e.g., Figure 2). In a funnel-shaped channel, however, the deposition triggered in the region where width

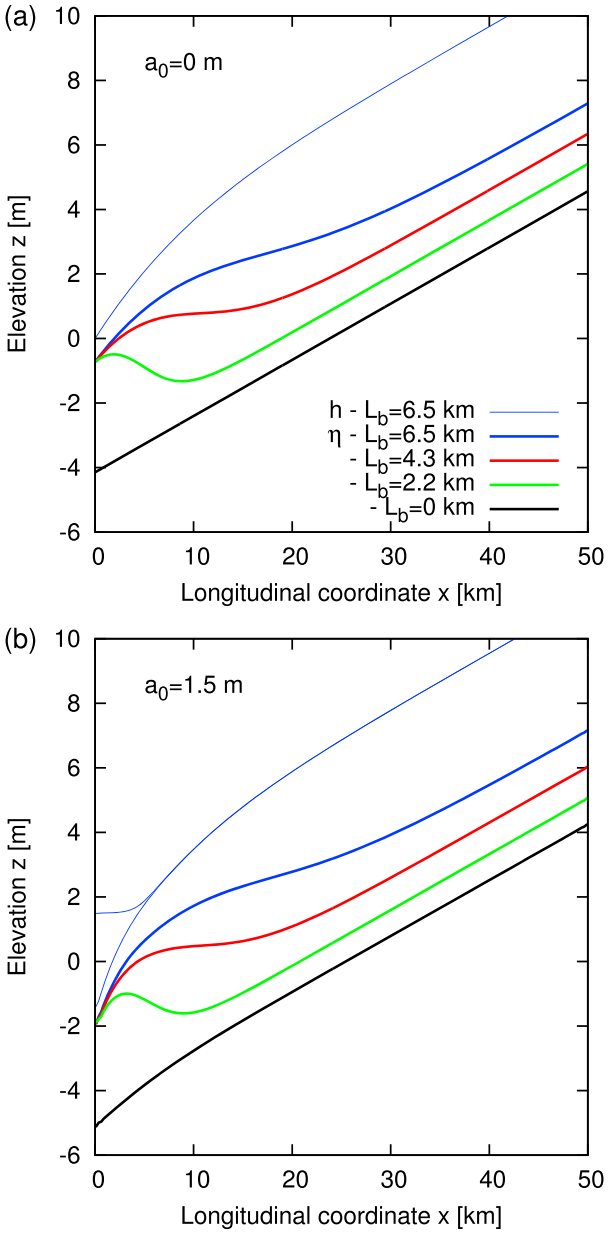

Figure 13. Equilibrium configurations of the bed and corresponding profiles of the free surface for the three estuaries depicted in Figure 12a, which are characterized by different values of the convergence length L_b. The limiting case of a constant width estuary ($L_b = 0$) is also plotted. (a) No tidal forcing; (b) a tidal oscillation is forced at the inlet with an amplitude $a_0 = 1.5$ m. The channels are filled with uniform sediment ($d_s = 0.1$ mm) and fed by a constant river discharge. The upstream river width and the sediment flux are prescribed employing the equilibrium relations of *Wilkerson and Parker* [2011] appropriate for single-thread sand-bed rivers. Input data: $r_B = 10.5$, $d_s = 0.1$ mm, $Q_u = 1000\ m^3/s$, $Q_{su} = 0.355\ m^3/s$, $L_b = 0, 2.2, 4.3$, and 6.5 km.

expands leads to a progressive seaward decrease of bed slope, in some cases developing even a counterslope (Figure 13). Only in a region close to the sea where the tidal strength and, therefore, tidal flushing grow, a seaward increase of depth and of slope occur, as observed for constant width channels (e.g., Figure 2).

The formation of a concave down estuary profile, with increasing slope toward the sea inlet, and an overall lowering of the bed, determining the net degradation of the river bed, are enhanced as the tidal amplitude increases (Figure 14c). Note that, as expected, the theoretical predictions of the asymptotic solution described in section 2.4 progressively deviate from the numerical solution as the tidal amplitude increases (not shown in Figure 14).

An important feature of the equilibrium bed profiles shown in Figures 13 and 14 is the remarkable decrease of the tidal length experienced by funneling estuaries (Figure 15). Although the dependence of the tidal length on variations of the tidal range and of the upstream river discharge are qualitatively similar to those observed for a constant width estuary (Figures 15a and 15b), the increase of cross-sectional area associated with funneling determines a significant progressive reduction of the tidal length. Moreover, for the same degree of convergence, an increase of the relative rate of width reduction (measured by r_B) implies a further reduction of the tidal length for relatively small values of r_B, followed by a moderate increase of the tidal length as the width ratio r_B becomes sufficiently large. The effects of changes in sediment diameter and friction coefficients are analogous to the case of prismatic channels.

4. Tidal Damping at Equilibrium

It is then worth analyzing our results in terms of the variation of the tidal range along the length of the estuary, in order to investigate how the morphological response of the estuary affects its

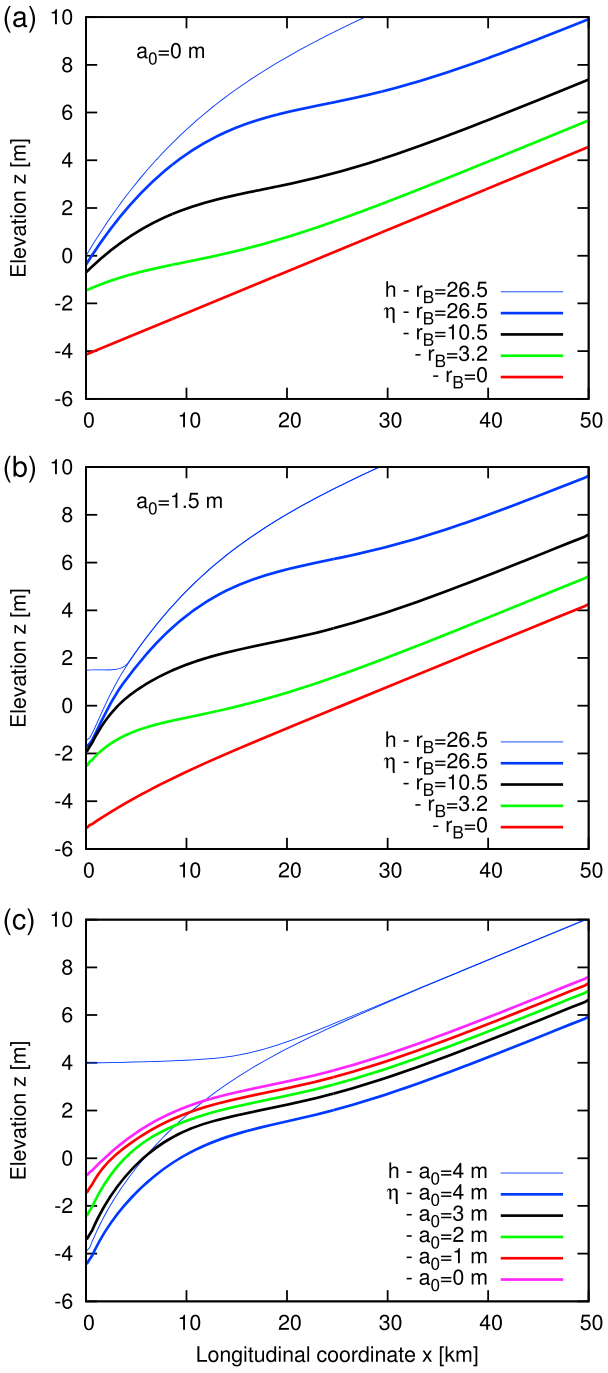

Figure 14. Equilibrium configurations of the bed and corresponding profiles of the free surface along the three estuaries depicted in Figure 12b, which are characterized by the same convergence length L_b and different values of relative width at the inlet r_B. (a) No tidal forcing; (b) a tidal oscillation is forced at the inlet with an amplitude $a_0 = 1.5$ m; (c) effect of variations of the tidal amplitude at the inlet ($r_B = 10.5$). The channels are fed with a constant flow discharge. The river width and the sediment flux are prescribed using the equilibrium relations of *Wilkerson and Parker* [2011] assuming a uniform grain size $d_s = 0.1$ mm. Input data: $L_b = 6.5$ km, $d_s = 0.1$ mm, $Q_u = 1000\ \mathrm{m^3/s}$, $Q_{su} = 0.355\ \mathrm{m^3/s}$.

hypersynchronous/hyposynchronous character. We then follow *Cai et al.* [2014] and define a damping coefficient δ quantifying the variation of the tidal range along the estuary:

$$\delta = \frac{1}{a}\frac{\mathrm{d}a}{\mathrm{d}X} \tag{20}$$

Here X is a normalized longitudinal coordinate, pointing landward and scaled by the reference tidal wavelength $\sqrt{gD}/\omega$, and a is a local tidal amplitude defined as half the tidal excursion. Needless to say, positive values of δ at the estuary mouth identify hypersynchronous estuaries and vice versa hyposynchronous estuaries are characterized by negative values of δ.

Results are reported in Figure 16 for a wide range of simulations performed for both constant width and convergent estuaries. Simulations differ also for the values of the tidal amplitude imposed at the estuary mouth of the upstream river discharge and of the degree of channel convergence. An interesting feature emerges: at equilibrium, none of the simulations leads to an amplification of the tidal range along the estuary. In few cases, the tidal range is approximately constant in the seaward portion of the estuary (the damping coefficient nearly vanishes), whereas in most of the simulations the final equilibrium configurations are characterized by a landward decrease of the tidal range, indicating the hyposynchronous character of the estuary. Note that this occurred invariably, in spite of the fact that, for some convergent estuaries, a transient hypersynchronous response was displayed during the evolution process under nonequilibrium conditions (dotted lines in Figures 16b and 16d).

5. Discussion

We can now provide answers to the questions we raised in section 1.

5.1. Existence of the Equilibrium Bed Profile

The main question we raised was: Does an equilibrium bed profile of an estuary

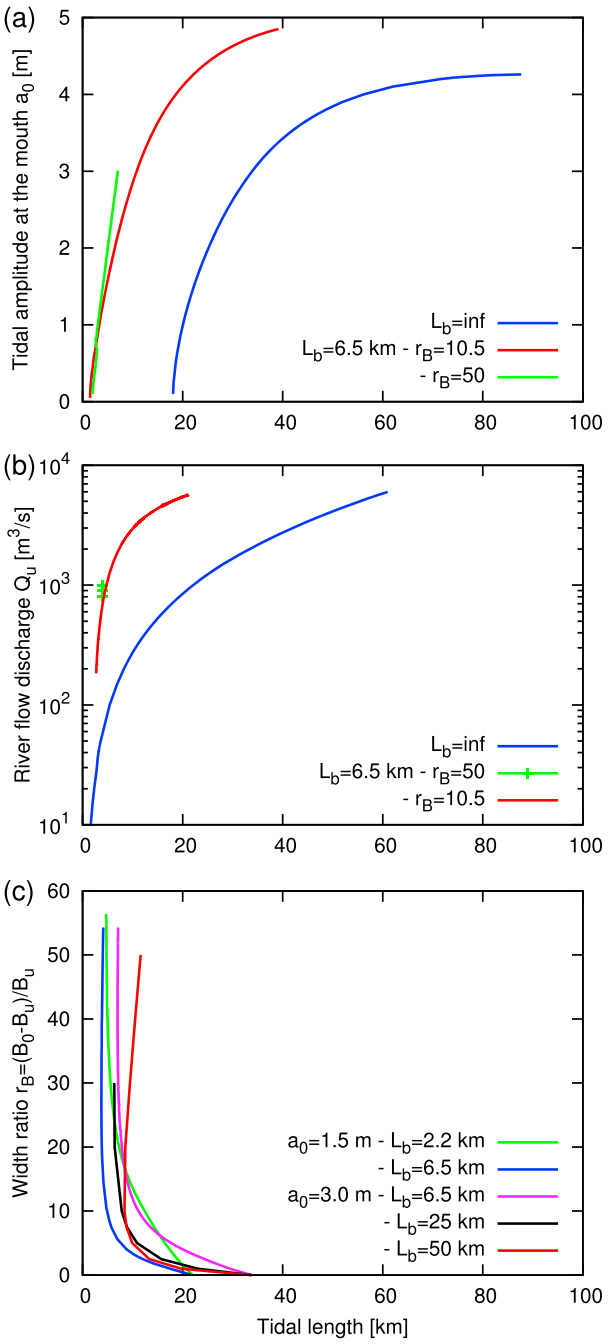

Figure 15. Variations of the tidal length for two convergent estuaries and a constant width estuary (blue line). (a) Effects of the tidal amplitude (Q_u = 1000 m^3/s); (b) effects of the upstream river discharge (a_0 = 1.5 m); (c) effects of degree of convergence (Q_u = 1000 m^3/s). The river width and the sediment discharge prescribed at the landward boundary have been determined employing the equilibrium relations of *Wilkerson and Parker* [2011], assuming a uniform grain size d_s = 0.1 mm.

exist for a given planform configuration? The answer is indeed positive, albeit it has been obtained under fairly idealized conditions, namely, steady fluvial and marine forcing, i.e., (i) constant fluvial discharge and sediment supply identified through formative conditions corresponding to the relations of *Wilkerson and Parker* [2011] and (ii) steady tidal oscillation imposed at the estuary mouth. In nature, neither fluvial forcing nor tidal forcing is steady: they undergo fluctuations associated with random variations of the hydrologic cycle, as well as with variations of the astronomical component of the tide. As a result, equilibrium may actually be defined only in statistical terms, which is not surprising in the light of the analogue problem extensively investigated in the fluvial case [see *Bolla Pittaluga et al.*, 2014, and references therein]. Also, note that the present analysis adopts a one-dimensional approach. Hence, the effect of morphological patterns at scales smaller than the estuary length (e.g., free and forced bars, dunes, and ripples) on the overall equilibrium of the estuary could be accounted for only through the friction coefficient and transport capacity of the stream. The presence of intertidal areas has also been neglected and therefore the results of this model should be taken with the proper caution before being applied to estuaries flanked by extensive floodplains/salt marshes. However, our model would still strictly apply to all the post-glacial rebound locations characterized by land surfaces that are elevated with respect to the maximum tidal level and creeks are incising in former tidal deposits, such as along the coast of the Gulf of Saint Lawrence, Canada. Moreover, a number of additional effects were not considered here, such as the downstream fining of sediment, the longitudinal variation of river flow discharge and sediment flux due to tributaries, and the presence of some geological constraints that might limit the bed erosion along the estuary.

5.2. Effect of Tidal Amplitude and River Flow Discharge

The second question we raised concerned the morphological response of an alluvial estuary to changes in the tidal range or in the incoming river flow and the corresponding sediment supply. We first checked

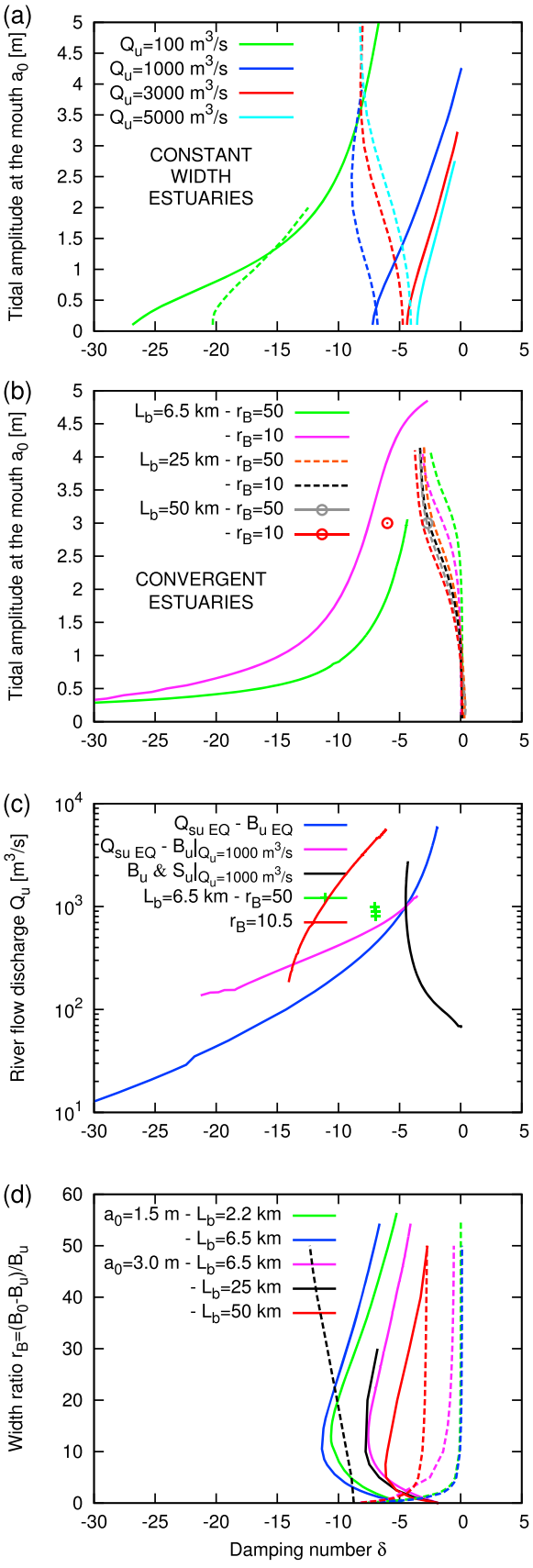

that the equilibrium configuration obtained in the absence of any tide did coincide with the uniformly sloping bed profile obtained under uniform flow conditions for given steady flow and sediment supply rates. Starting from the latter configuration and increasing the tidal oscillation for given fluvial forcing, we found that concave down equilibrium bed profiles developed through most of the estuary. Progressively higher bed slope at the mouth, as well as increasing bed degradation in the river-dominated portion of the estuary were associated with increasing values of the tidal forcing amplitude. This trend is due to the nonlinear dependence of the sediment transport rate on the speed of tidal currents. The increasing slope at the mouth is achieved through a scouring process arising from the need to limit the asymmetry of flow velocity between ebb and flood phases such that, at equilibrium, the net sediment flux driven by the tide is directed seaward and equal to the riverine sediment discharge (see Figure 2b). Conversely, decreasing the fluvial forcing (flow and sediment transport rates) for given tidal conditions was shown to produce larger bed slopes and smaller flow depths in the fluvial-dominated reach, a consequence of the morphological equilibrium constraint imposed at the landward boundary.

Figure 16. Variations of the damping coefficient δ at the estuary mouth for constant width and convergent estuaries. The dotted lines represent the cases of estuaries with a prescribed (and fixed) constant bed slope, whereas the continuous lines represent the cases of estuaries at equilibrium. (a) Effects of the tidal amplitude for different values of the upstream river discharge in constant width estuaries; (b) effects of the tidal amplitude with different degrees of convergence ($Q_u = 1000\,m^3/s$); (c) effects of the upstream river discharge in a constant width (blue, pink, and black lines) and convergent (green and red lines) estuaries ($a_0 = 1.5\,m$); (d) effects of degree of convergence ($Q_u = 1000\,m^3/s$). The river width and the sediment discharge prescribed at the landward boundary have been determined employing the equilibrium relations of *Wilkerson and Parker* [2011], assuming a uniform grain size $d_s = 0.1$ mm.

5.3. Location of the Fluvial-Marine Transition

The third issue we raised concerned the identification of the fluvial-marine transition and its dependence on the fluvial and tidal forcing. A measure of the extension of the tide-dominated region was introduced, defining a tidal length as the distance from the inlet where some property of the tidal wave is reduced to some small percentage of its value at the inlet. Choosing this property as either the tidal amplitude, a, or the relative tidal prism, P_{rel}, leads to quite similar values of the tidal length. The tidal length decreases monotonically as the river discharge, and the associated sediment supply are decreased such that the river keeps in morphological equilibrium. In contrast, the tidal length increases monotonically if, for a fixed river discharge and tidal amplitude, the sediment flux is progressively reduced with respect to its equilibrium value.

These results are readily understood by analyzing how the relevant hydrodynamic parameters vary as the upstream sediment supply is increased above (or decreased below) the transport capacity of the river. Using Chézy law for the uniform flow and *Engelund and Hansen* [1967] relationship to estimate the sediment transport capacity of the river, we immediately find

$$\frac{S}{S_u} = \left(\frac{Q_s}{Q_{su}}\right)^{20/33}, \quad \frac{D}{D_u} = \left(\frac{Q_s}{Q_{su}}\right)^{-2/11}, \tag{21}$$

where the subscript u denotes the reference uniform conditions characterizing the landward river reach. Equation (21) suggests that, if the upstream sediment supply increases, the equilibrium constraints imply that the river slope also increases and the flow becomes shallower (more dissipative), thus damping the propagation of the tide in the landward direction. On the contrary, decreasing the sediment supply leads to a milder equilibrium slope and a deeper flow, favoring the landward propagation of the tide.

The effects of grain size or width variations can be similarly explained. Indeed, increasing the sediment size implies higher slopes, consistently with the relation of *Wilkerson and Parker* [2011], which predicts a power law dependence of the equilibrium bed slope on sediment size with exponent 0.691. On the other hand, it can be easily demonstrated that the longitudinal bed slope and flow depth depend on width according to the following relations:

$$\frac{S}{S_u} = \left(\frac{B}{B_u}\right)^{2/7}, \quad \frac{D}{D_u} = \left(\frac{B}{B_u}\right)^{-24/35}, \tag{22}$$

indicating that the morphological effects of channel widening/narrowing follow a trend analogous to that associated with increasing/decreasing sediment discharge: tide propagation is favored (leading to larger tidal lengths) both decreasing the sediment supply and narrowing the river (Figure 8). In the case of funnel-shaped estuaries aggradation is triggered by channel widening and tidal effects are such to enhance the slope at the inlet and the net degradation of the river bed. More significantly, the tidal length decreases strongly as a result of the seaward increase of cross-sectional area associated with funneling. This finding is not surprising in the light of Figure 8. Indeed, funneling is equivalent to a progressive seaward increase of channel width, which we have seen to imply a tendency to reduce the tidal length.

5.4. No Amplification of the Tidal Wave at Equilibrium

Finally, results presented in section 4 suggest that a simple necessary condition that must be satisfied by an alluvial estuary in morphological equilibrium might be that no amplification is experienced by the tidal wave propagating landward. We cannot claim generality for this statement which is based on numerical simulations. However, some theoretical substantiation of the latter result comes from the theories of *Seminara et al.* [2010, 2012] where it was shown that, at least for small-amplitude tidal forcing, at equilibrium the tidal wave cannot experience any amplification. Further substantiation based on field observations and possibly on theoretical work will be needed in order to make the validity of the above criterion conclusively assessed.

5.5. Limitations of the Numerical Model

Needless to say a number of further features of real estuaries, ignored in the present analysis, will also require attention in the future. In particular, we have neglected the presence of overtides at the inlet of the estuary, an ingredient that can be easily incorporated in the present model. Moreover, the effects of wave action and gravitational circulations driven by salinity and density gradients were not accounted for. While the latter motion is likely to have minor morphological consequences, the role of wave motion in wave-dominated environments may alter the picture arising from the present work, whose validity is strictly

restricted to estuaries where the tide and the riverine action are the dominant forcing mechanisms. The dependence of estuarine equilibrium on the tidal and fluvial "climates" will also deserve attention. Previous work on the tidal inlets of Venice lagoon [*Tambroni and Seminara*, 2006] has shown that the tidal motion through those inlets undergoes repetitive seasonal fluctuations which, in turn, generate fluctuations of the intensity and direction of sediment exchange through the inlet. The response of estuarine equilibrium to such fluctuations needs to be understood. This, notwithstanding the knowledge of the equilibrium configuration of the bed profile along the estuary, might play a crucial role in the interpretations of sedimentary deposits in tide-dominated environments. Indeed, our results can indicate how the depositional structure of different systems is linked to the type of forcings acting on the estuary and the sediment grain size. Rivers with larger tidal range, larger formative water discharge or smaller characteristic grain size are more likely to have a larger tidal length, since its equilibrium value is larger. In these rivers, the reach in which cyclic tidal deposits, such as rhythmites, can be found would extend further upstream.

6. Conclusions

We investigated, through a one-dimensional numerical model, the evolution of the longitudinal bed profile of an estuary, with fixed planform configuration, subject to given tidal forcing at the mouth and prescribed values of water and sediment supply from the river. The main conclusions of this paper can be summarized as follows:

1. The model is able to describe a wide class of settings ranging from tidally dominated estuaries to fluvially dominated estuaries. In the latter case, the solution is found to compare satisfactory with the analytical asymptotic solution recently derived by *Seminara et al.* [2012], under the hypothesis of fairly small tidal oscillations.
2. Simulations indicate that the investigated system always moves toward an equilibrium configuration in which the net sediment flux in a tidal cycle keeps constant throughout the estuary and equal to the constant sediment flux delivered by the river.
3. The bed equilibrium profile of the estuarine channel is characterized by two distinct regions: a steeper seaward reach, dominated by the tide, and a less steep upstream reach, dominated by the river and characterized by the undisturbed riverine bed slope.
4. In the case of constant width, for a given river discharge, the length of the tidal reach (equilibrium tidal length) increases quite rapidly with tidal amplitude, up to some threshold value of the tidal amplitude above which the length of the estuary becomes comparable with the length of the tidal wave. Furthermore, for a given tidal amplitude, equilibrium tidal length decreases monotonically as the formative river discharge and the associated sediment supply are decreased. In contrast, it increases monotonically if, for a fixed river discharge and tidal amplitude, the sediment flux (or the river width) is progressively reduced with respect to its equilibrium value. Finally, increasing grain size leads to shorter tidal lengths at equilibrium.
5. In the case of funnel-shaped estuaries, the effect of an increasing channel convergence is to induce bed aggradation close to the inlet. Moreover, the equilibrium tidal length decreases strongly as a result of the seaward increase of cross-sectional area associated with funneling.
6. Finally, our results suggest that alluvial estuaries in morphological equilibrium cannot experience any amplification of the tidal wave propagating landward. Hence, hypersynchronous alluvial estuaries cannot be in equilibrium.

Acknowledgments
Partial funding has been provided to Stefano Lanzoni by the University of Padua, within the project "Morphodynamics of marsh systems subject to natural forcings and climate changes." Alberto Canestrelli was supported by NSF award FESD/EAR-1135427. The data reported in the figures can be made available at request by the corresponding author (M. Bolla Pittaluga).

References

Bolla Pittaluga, M., R. Luchi, and G. Seminara (2014), On the equilibrium profile of river beds, *J. Geophys. Res. Earth Surf.*, *119*, 317–332, doi:10.1002/2013JF002806.

Cai, H., H. H. G. Savenije, and M. Toffolon (2014), Linking the river to the estuary: Influence of river discharge on tidal damping, *Hydrol. Earth Syst. Sci.*, *18*, 287–304, doi:10.5194/hess-18-287-2014.

Canestrelli, A., and E. F. Toro (2012), Restoration of the contact surface in FORCE-type centered schemes II: Non conservative one- and two-layer two-dimensional shallow water equations, *Adv. Water Resour.*, *47*, 76–87.

Canestrelli, A., N. Siviglia, M. Dumbser, and E. F. Toro (2009), Well-balanced high-order non-conservative centered schemes for shallow water equations with fix and mobile bed, *Adv. Water Resour.*, *32*, 834–844, doi:10.1016/j.advwatres.2009.02.006.

Canestrelli, A., N. Siviglia, M. Dumbser, and E. F. Toro (2010), Well-balanced high-order centered schemes on unstructured meshes for shallow water equations with fixed and mobile bed, *Adv. Water Resour.*, *33*(3), 291–303.

Canestrelli, A., S. Fagherazzi, and S. Lanzoni (2012), A mass-conservative centered finite volume model for solving two-dimensional two-layer shallow water equations for fluid mud propagation over varying topography and dry areas, *Adv. Water Resour.*, *40*, 54–70.

Canestrelli, A., S. Lanzoni, and S. Fagherazzi (2014), One-dimensional numerical modeling of the long-term morphodynamic evolution of a tidally dominated estuary: The Lower Fly River (Papua New Guinea), *Sediment. Geol.*, *301*, 107–119.

D'Alpaos, A., S. Lanzoni, M. Marani, and A. Rinaldo (2010), On the tidal prism-channel area relations, *J. Geophys. Res.*, *115*, F01003, doi:10.1029/2008JF001243.

Dalrymple, R. W., and K. Choi (2007), Morphologic and facies trends through the fluvial-marine transition in tide-dominated depositional systems: A schematic framework for environmental and sequence-stratigraphic interpretation, *Earth Sci. Rev.*, *81*(3-4), 135–174, doi:10.1016/j.earscirev.2006.10.002.

Dalrymple, S. W., B. A. Zaitlin, and R. Boyd (1992), Estuarine facies model: Conceptual basis and stratigraphic implications, *J. Sediment. Petrol.*, *62*(6), 1130–1146.

Engelund, F., and E. Hansen (1967), *A Monograph on Sediment Transport in Alluvial Streams*, Danish Tech. Press, Copenhagen.

Exner, F. M. (1925), Uber die Wechselwirkung zwischen Wasser und Geschiebe in Flussen, Sitzungsber, *Akad. Wiss. Wien, Math. Naturwiss. Kl.*, *Abt. 2A*(134), 165–18.

Friedrichs, C. T. (1995), Stability shear stress and equilibrium cross-sectional geometry of sheltered tidal channels, *J. Coastal Res.*, *11*(4), 1062–1074.

Friedrichs, C. T., and D. G. Aubrey (1994), Tidal propagation in strongly convergent channels, *J. Geophys. Res.*, *99*(C2), 3321–3336.

Friedrichs, C. T., and O. S. Madsen (1992), Nonlinear diffusion of the tidal signal in frictionally dominated embayments, *J. Geophys. Res.*, *97*(C4), 5637–5650.

Hansen, D. V., and M. Rattray (1966), New dimensions in estuary classification, *Limnol. Oceanogr.*, *11*(3), 319–326.

Huijts, K. M. H., H. M. Schuttelaars, H. E. de Swart, and C. T. Friedrichs (2009), Analytical study of the transverse distribution of along-channel and transverse residual flows in tidal estuaries, *Cont. Shelf Res.*, *29*(1), 89–100, doi:10.1016/j.csr.2007.09.007.

Jay, D. A. (1991), Green's law revisited: Tidal long-wave propagation in channels with strong topography, *J. Geophys. Res.*, *96*, 20,585–20,598.

Langbein, W. B. (1963), The hydraulic geometry of a shallow estuary, *Bull. Int. Assoc. Sci. Hydrol.*, *8*, 84–94.

Lanzoni, S., and G. Seminara (1998), On tide propagation in convergent estuaries, *J. Geophys. Res.*, *103*(C13), 30,793–30,812.

Lanzoni, S., and G. Seminara (2002), Long-term evolution and morphodynamic equilibrium of tidal channels, *J. Geophys. Res.*, *107*, C13001, doi:10.1029/2000JC000468.

Mirick, R. M., and L. B. Leopold (1963), *Hydraulic Geometry of a Small Tidal Estuary*, Geol. Surv. Prof. Pap., 422-B, Washington, D. C.

Perillo, G. M. E. (1995), *Geomorphology and Sedimentology of Estuaries. Developments in Sedimentology*, vol. 53, Elsevier Science B.V., Amsterdam.

Pethick, J. (1984), *An Introduction to Coastal Geomorphology*, Edward Arnold, London.

Roelvink, J. A. (2006), Coastal morphodynamic evolution techniques, *Coastal Eng.*, *53*, 277–287.

Savenije, H. H. G. (2005), *Salinity and Tides in Alluvial Estuaries*, Elsevier, Amsterdam.

Savenije, H. H. G., and E. J. M. Veling (2005), Relation between tidal damping and wave celerity in estuaries, *J. Geophys. Res.*, *110*, C04007, doi:10.1029/2004JC002278.

Schuttelaars, H. M., and H. E. de Swart (2000), Multiple morphodynamic equilibria in tidal embayments, *J. Geophys. Res.*, *105*(C10), 24,105–24,118.

Seminara, G., S. Lanzoni, N. Tambroni, and M. Toffolon (2010), How long are tidal channels?, *J. Fluid Mech.*, *643*, 479–494.

Seminara, G., M. Bolla Pittaluga, and N. Tambroni (2012), Morphodynamic equilibrium of tidal channels, in *Environmental Fluid Meechanics- Memorial Volume in Honour of Prof. Gerhard Jirka, Karslrhue (Gemany)*, edited by W. Rodi and M. Uhlmann, pp. 153–174, Taylor and Francis, CRC Press/Balkema, 3–4 June 2011.

Tambroni, N., and G. Seminara (2006), Are inlets responsible for the morphological degradation of Venice Lagoon?, *J. Geophys. Res.*, *111*, F03013, doi:10.1029/2005JF000334.

Tambroni, N., and G. Seminara (2009), On the theoretical basis of O'Brien-Jarret-Marchi law for tidal inlets and tidal channels, paper presented at 6th IAHR Symposium on River, Coastal and Estuarine Morphodynamics, pp. 329–335, Taylor Francis/Balkema, Santa Fe, Argentina, Calif., 21-25 Sept.

Tambroni, N., M. Bolla Pittaluga, and G. Seminara (2005), Laboratory observations of the morphodynamic evolution of tidal channels and tidal inlets, *J. Geophys. Res.*, *110*, F04009, doi:10.1029/2004JF000243.

Todeschini, I., M. Toffolon, and M. Tubino (2008), Long-term morphological evolution of funnelshape tide-dominated estuaries, *J. Geophys. Res.*, *113*, C05005, doi:10.1029/2007JC004094.

Toffolon, M., and S. Lanzoni (2010), Morphological equilibrium of short channels dissecting the tidal flats of coastal lagoons, *J. Geophys. Res.*, *115*, F04036, doi:10.1029/2010JF001673.

van der Wegen, M., A. Dastgheib, and J. A. Roelvink (2010), Morphodynamic modeling of tidal channel evolution in comparison to empirical PA relationship, *Coastal Eng.*, *57*(9), 827–837, doi:10.1016/j.coastaleng.2010.04.003.

Wilkerson, G., and G. Parker (2011), Physical basis for quasi-universal relationships describing bankfull hydraulic geometry of sand-bed rivers, *J. Hydraul. Eng.*, *137*(7), 739–753.

Wright, L. D., J. M. Coleman, and B. G. Thom (1973), Processes of channel development in a high-tide-range environment: Cambridge Gulf-Ord River Delta, Western Australia, *J. Geol.*, *81*, 15–41.

Zhou, Z., M. Olabarrieta, L. Stefanon, A. D'Alpaos, L. Carniello, and G. Coco (2014), A comparative study of physical and numerical modeling of tidal network ontogeny, *J. Geophys. Res. Earth Surf.*, *119*, 892–912, doi:10.1002/2014JF003092.